Nuclear Theory'21
ed. V. Nikolaev, Heron Press, Sofia, 2002

Systematic Study of Deformed Nuclei at the Drip Lines and Beyond

M.V. Stoitsov[1,3], **J. Dobaczewski**[2], **W. Nazarewicz**[3], **and S. Pittel**[4]

[1]Institute of Nuclear Research and Nuclear Energy, Bulgarian Academy of Sciences, Sofia 1784, Bulgaria

[2]Institute of Theoretical Physics, Warsaw University, Hoża 69, PL-00-681 Warsaw, Poland

[3]Joint Institute for Heavy Ion Research, Oak Ridge, Tennessee 37831
Department of Physics, University of Tennessee, Knoxville, Tennessee 37996
Physics Division, Oak Ridge National Laboratory, Oak Ridge, Tennessee 37831

[4]Bartol Research Institute, University of Delaware, Newark, Delaware 19716

Abstract.

An improved prescription for choosing a Transformed Harmonic Oscillator (THO) basis for use in configuration-space Hartree-Fock-Bogoliubov (HFB) calculations is presented. The new HFB+THO framework that follows accurately reproduces the results of coordinate-space HFB calculations for spherical and axially-deformed nuclei, including those that are weakly bound. Furthermore, it is fully automated, facilitating its use in systematic investigations of large sets of nuclei throughout the periodic table. As a first application, we have carried out calculations using the Skyrme Force SkLY4 and volume pairing for all even-even nuclei from proton drip-line to neutron drip-line having proton numbers $Z = 4, 6, 8, ..., 108$. We focus on those nuclei very near the drip lines and find that there exist numerous particle-bound even-even nuclei (i.e., nuclei with negative Fermi energies) that have negative two-proton or two-neutron separation energies. This phenomenon, which was earlier noted for light nuclei only, is now seen to occur in several diverse regions of the periodic table.

1 Introduction

The development of experimental facilities that accelerate radioactive ion beams [1–4] has opened up a window to many nuclei that were heretofore inaccessible. With these new facilities and the new detector technology that is accompanying them, it is becoming possible to study the properties of nuclei very far from the valley of beta stability, all the way out to the particle "drip lines".

Much work is now in progress to develop appropriate theoretical tools for describing nuclei in these exotic regimes. A proper theoretical description of such weakly-bound systems requires a careful treatment of the asymptotic part of the nucleonic density. An appropriate framework for these calculations is Hartree-Fock-Bogoliubov (HFB) theory, solved in coordinate representation [5–7]. This method has been used extensively in the treatment of spherical systems but is much more difficult to implement for systems with deformed equilibrium shapes [8–10].

In the absence of reliable coordinate-space solutions to the deformed HFB equations, it is useful to consider instead the configuration-space approach, where by the HFB solution is expanded in a single-particle basis. One approach has been to use a truncated basis composed partly of discrete localized states and partly of discretized continuum and oscillating states [8, 9, 11]. Because of the technical difficulties in implementing this method, it has typically been restricted to include states in the continuum up to at most several MeV. As a consequence, such an approach should not be able to describe adequately the spatial properties of nuclear densities at large distances.

An alternative possibility is to expand in a basis of spatially localized states. Expansion in a harmonic oscillator (HO) basis is particularly attractive because of the simple properties of oscillator states. There have been many configuration-space HFB+HO calculations reported, either employing Skyrme forces or the Gogny effective interaction [12–15], or using a relativistic Lagrangian [16, 17]. This methodology has proven particularly useful when treating nuclei in or near the valley of stability. For nuclei at the drip lines, however, the HFB+HO expansion converges slowly as a function of the number of oscillator shells [7], producing wave functions that decrease too steeply at large distances. The resulting densities, especially in the pairing channel, are too small in the outer region and do not reflect correctly the pairing correlations of these weakly-bound nuclei.

A related approach that has recently been proposed is to instead expand the quasiparticle HFB wave functions in a complete set of transformed harmonic oscillator (THO) basis states [18–20], obtained by applying a local-scaling coordinate transformation (LST) [21–23] to the standard HO basis. The THO basis preserves many useful properties of the HO wave functions, including its simplicity in numerical algorithms, while at the same time permitting us to incorporate the appropriate asymptotic behavior of nuclear densities.

Applications of this new HFB+THO methodology have been reported both in the non-relativistic [18] and relativistic domains [20]. In all of these calculations, specific global parameterizations were employed for the scalar LST function that defines the THO basis. There are several limitations in such an approach, however. On the one hand, any global parameterization of the LST function will of necessity modify properties throughout the entire nuclear volume, in order to improve the asymptotic density at large distances. This is not desirable, however, since the HFB+HO results are usually reliable in the nuclear interior, even for weakly-bound systems. In addition, because of the need to introduce matching conditions between the interior and exterior regions, a global LST function will invariably have a very complicated behavior, especially around the classical turning point, making it difficult to simply parameterize it. Perhaps most importantly, the minimization procedure that is needed in such an approach to optimally define the basis parameters is computationally very time consuming, especially when a large number of shells are included, making it very difficult to apply the method systematically to nuclei across the periodic table.

In the present work, we propose a new prescription for choosing the THO basis. For a given nucleus, our new prescription requires as input the results from a relatively simple HFB+HO calculation, with no variational optimization. The resulting THO basis leads to HFB+THO results that almost exactly reproduce the coordinate-space HFB results for spherical [6] and axially deformed [11] nuclei and are of comparable quality to those of the former, more complex, HFB+THO methodology.

Because the new prescription requires no variational optimization of the LST function, it can be readily applied in systematic studies of nuclear properties. As the first such application, we have carried out a detailed study of nuclei at the two-particle proton and neutron drip lines throughout the periodic table, using the Skyrme force SkL4 and volume pairing [18].

The structure of the paper is the following. In Section 2, we briefly review the HFB theory, noting several features particular to its coordinate and configurational representation. In Section 3, we introduce the THO basis and then formulate our new prescription for the LST function. The results of systematic calculations of all chains of even-even nuclei from Ne to Pu are reported in Section 4, with special emphasis on those nuclei that are at the drip lines and just beyond. Conclusions and thoughts for the future are presented in Section 5.

2 Overview of Hartree-Fock-Bogoliubov Theory

In this section, we review the basic ingredients of Hartree-Fock-Bogoliubov (HFB) theory, both in coordinate representation and in configuration space. Since HFB theory is by now a standard tool in nuclear structure, we keep the presentation brief and refer the reader to Ref. [24] for more details.

HFB is a variational theory that treats in a unified fashion mean field and pairing correlations. The HFB equations can be written in matrix form as

$$\begin{pmatrix} h-\lambda & \Delta \\ -\Delta^* & -h^*+\lambda \end{pmatrix} \begin{pmatrix} U_n \\ V_n \end{pmatrix} = E_n \begin{pmatrix} U_n \\ V_n \end{pmatrix} , \tag{1}$$

where E_n are the quasiparticle energies, λ is the chemical potential, $h = t+\Gamma$ and Δ are the Hartree Fock hamiltonian and the pairing potential, respectively, and U_n and V_n are the upper and lower components of the quasiparticle wave functions. These equations are solved subject to constraints on the average numbers of neutrons and protons in the system, which determine the two corresponding chemical potentials, λ_n and λ_p.

In coordinate representation, the HFB approach consists in solving (1) as a set of integro-differential equations with respect to the amplitudes $U(E_n, \mathbf{r})$ and $V(E_n, \mathbf{r})$, both of which are functions of the position coordinate $\mathbf{r}$. The resulting density matrix and pairing tensor then read

$$\begin{aligned} \rho(\mathbf{r},\mathbf{r}') &= \sum_{0\le E_n\le E_{\max}} V^*(E_n,\mathbf{r})V(E_n,\mathbf{r}') , \\ k(\mathbf{r},\mathbf{r}') &= \sum_{0\le E_n\le E_{\max}} V^*(E_n,\mathbf{r})U(E_n,\mathbf{r}') . \end{aligned} \tag{2}$$

Typically, the HFB continuum is discretized in this approach by putting the system in a large box with appropriate boundary conditions [7].

In the configurational approach, the HFB equations are solved by matrix diagonalization within a chosen set of single-particle basis wave functions ψ_α with appropriate symmetry properties. In this sense, the amplitudes U_n and V_n entering Eq. (1) may be thought of as expansion coefficients of the quasiparticle states in the chosen basis. The nuclear characteristics of interest are determined from the density matrix and pairing tensor

$$\begin{aligned} \rho(\mathbf{r},\mathbf{r}') &= \sum_{\alpha\beta} \rho_{\alpha\beta}\psi_\alpha(\mathbf{r})\psi^*_\beta(\mathbf{r}') , \\ k(\mathbf{r},\mathbf{r}') &= \sum_{\alpha\beta} k_{\alpha\beta}\psi_\alpha(\mathbf{r})\psi_\beta(\mathbf{r}') , \end{aligned} \tag{3}$$

which are expressed in terms of the basis states ψ_α and the associated basis matrix elements

$$\begin{aligned} \rho_{\alpha\beta} &= \sum_{0\le E_n\le E_{\max}} V^*_{\alpha n}(E_n)V_{\beta n}(E_n) , \\ k_{\alpha\beta} &= \sum_{0\le E_n\le E_{\max}} V^*_{\alpha n}(E_n)U_{\beta n}(E_n) . \end{aligned} \tag{4}$$

In configuration-space calculations, all quasiparticle states have discrete energies E_n.

The results from configuration-space HFB calculations should be identical to those from the coordinate-space approach when all the states from a complete single-particle basis ψ_α are taken into account. Of course, this is never possible. In the presence of truncation, it is essential that the basis produce rapid convergence, so that reliable results can be obtained within the computational limitations on the number of basis states that can be included.

3 The Transformed Harmonic Oscillator Basis

In the present study, we carry out HFB calculations in configuration space, expanding in a transformed harmonic oscillator (THO) basis. This basis was originally introduced in Refs. [18–20], and we refer the reader to Ref. [18] for details concerning the use of the deformed THO basis and for a discussion of the cutoff procedure that is used to perform the summations in Eq. (4). We also refer the reader to an interesting new application of the THO basis to one-dimensional problems of interest in molecular physics [25].

As noted earlier, all previous calculations using the THO basis in HFB calculations employed a global parameterization of the LST function that defined the basis. In the following subsections, we develop a new and improved form for the transformation, which we then use in the HFB+THO calculations to be reported in Section 5.

3.1 Comparison of Coordinate-Space HFB Calculations and Configuration-Space HFB+HO Calculations

The main differences between the results of coordinate-space HFB calculations and those from configuration-space HFB+HO calculations can be seen in plots of the corresponding local density distributions. A typical example is shown in Figure 1, where the densities and their logarithmic derivatives from coordinate-space HFB calculations (solid lines) are compared with those from a configurational HFB+HO calculation. Although the calculations were done for a specific spherical nucleus and Skyrme interaction, the features exhibited are generic. Note that the coordinate-space HFB calculations were carried out in the box of 30 fm, so that the logarithmic derivative of the density obtained in that calculation shows a sudden drop near the box edge.

Invariably, the logarithmic derivative ρ'/ρ associated with the coordinate-space HFB solution shows a well-defined minimum near some point $R_{\min}$ in the asymptotic region, after which it smoothly approaches a constant value k=2κ, where

$$\kappa = \sqrt{2m(E_{\min} - \lambda)/\hbar^2}\,, \tag{5}$$

is associated with the HFB asymptotic behavior for the lowest quasiparticle state that has the corresponding quasiparticle energy $E_{\min}$ (see Ref. [6]). This property is clearly seen in the upper panel of Figure 1. One can also see that the

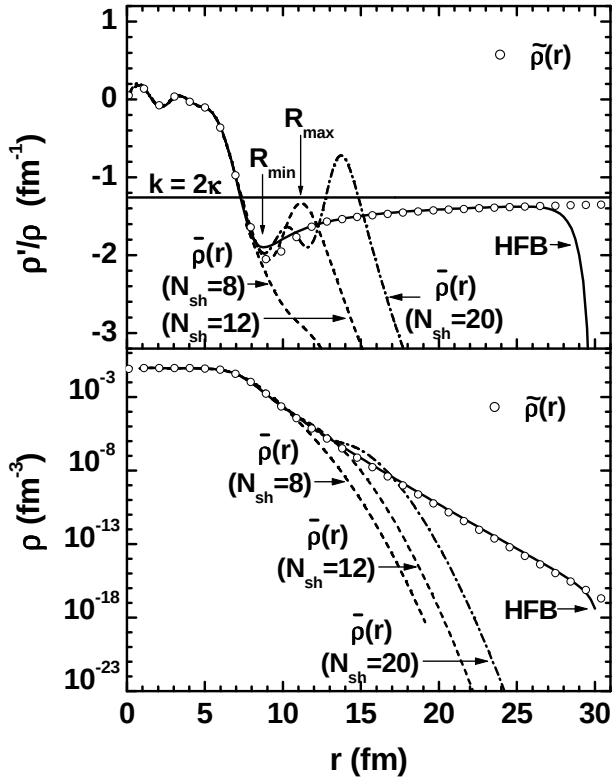

Figure 1. Logarithmic derivative of the density (upper panel), and the density in logarithmic scale (lower panel), as functions of the radial distance. The coordinate-space HFB results (solid line) are compared with those for the HFB+HO method (denoted $\bar{\rho}$) with $N_{\rm sh}$ = 8, 12 and 20 HO shells, as well with the approximation (denoted $\tilde{\rho}$) given by Eq. (11) (small circles).

HFB+HO densities and logarithmic derivatives are in almost perfect agreement with the coordinate-space results up to (or around) the distance $R_{\rm min}$. We conclude, therefore, that the HFB+HO densities are numerically reliable up to that point.

Moreover, the HFB value of the density decay constant k=2κ, when calculated from Eq. (5), is also correctly reproduced by the HFB+HO results. It is not possible to distinguish between the values of k that emerge from the coordinate-space and harmonic-oscillator HFB calculations, both values being shown by the same line in the upper panel of Figure 1.

Soon beyond the point $R_{\rm min}$, the HFB+HO density begins to deviate dramatically from that obtained in the coordinate-spce calculation. For relatively

small number of harmonic oscillator shells $N_{\rm sh}$ the logarithmic derivative of the HFB+HO density goes asymptotically to zero following the gaussian behavior of the harmonic oscillator basis. The resulting HFB+HO density does not develop a minimum around the point $R_{\rm min}$ as in the case of $N_{\rm sh} = 8$ results shown in the upper panel of Figure 1. When the number of harmonic oscillator shells $N_{\rm sh}$ is increased the HFB+HO solution tries to capture the correct density assymptotics. Due to the gaussian asymptotic of the basis, however, the logarithmic derivative of the HFB+HO density only develops oscillations around the exact solution, as can be seen by comparing the $N_{\rm sh} = 12$ and 20 results in the upper panel of Figure 1. As a result, the logarithmic derivative of the HFB+HO density is very close to the coordinate-space result around the mid point $R_m = (R_{\rm max} - R_{\rm min})/2$, where $R_{\rm max}$ is the position of the first maximum of the logarithmic derivative after $R_{\rm min}$.

In summary, the following HFB+HO quantities agree with the coordinate-space HFB results: *(i)* the value of the density decay constant k; *(ii)* the local density up to the point $R_{\rm min}$ where the logarithmic derivative ρ'/ρ shows a clearly-defined minimum; *(iii)* the actual value of this point $R_{\rm min}$; *(iv)* the value of the logarithmic derivative of the density at the point R_m defined above. In fact, the last of the above is not established nearly as firmly as the first three; nevertheless, we shall make use of it in developing our new formulation of the HFB+THO method.

Beyond the point R_m, the HFB+HO solution fails to capture the physics of the coordinate-space results, especially in the far asymptotic region. It is this incorrect large-r behavior that we now try to cure by introducing the THO basis.

3.2 Approximation to the Coordinate-Space HFB Local Densities

Our goal is to try to find an approximation to the *exact* (coordinate-space) HFB density that is based only on information contained in the HFB+HO results. Towards that end, we make use of the WKB asymptotic solution of the single-particle Schrödinger equation for a given potential $V(r)$, assuming that beyond the classical turning point only the state with the lowest decay constant k=2κ contributes to the local density. Under this assumption, the logarithmic derivative of the density can be written as

$$\left.\frac{\rho'(r)}{\rho(r)}\right|_{r\longrightarrow\infty} = -\frac{2}{r} - 2\sqrt{\kappa^2+\mathcal{V}} - \frac{1}{2}\frac{\mathcal{V}'}{\kappa^2+\mathcal{V}}, \tag{6}$$

where the first term comes from the three-dimensional volume element, while the next two correspond to the first- and second-order WKB solutions [26]. The reduced potential $\mathcal{V}$,

$$\mathcal{V}(r) = \frac{2m}{\hbar^2}V(r) = \mathcal{V}_N + \frac{\ell(\ell+1)}{r^2} + \frac{2m}{\hbar^2}\frac{Ze^2}{r}, \tag{7}$$

is the sum of the nuclear, centrifugal, and Coulomb (for protons) contributions, where ℓ is the multipolarity of the particular state.

In practical applications, it turns out that near R_m the next-to-lowest quasiparticle states still contribute to the local density ρ, in a way that may be more important than the second-order WKB term shown in Eq. (6). Moreover, in deformed nuclei the quasiparticle states do not have good total angular momentum ℓ, so that several quasiparticles may contribute to the asymptotic density depending on their ℓ-contents and the value of κ. Therefore, we need a practical prescription to fix a reasonable approximate asymptotic form of the density with minimal numerical effort but high reliability. This goal can be achieved by using in (6) a reduced potential of the form

$$\mathcal{V}(r) = \frac{C}{r^2} + \frac{2m}{\hbar^2}\frac{Ze^2}{r}, \tag{8}$$

where the nuclear part $\mathcal{V}_N$ (which is small around and beyond R_m) is neglected, and the coefficient C is allowed to differ from its centrifugal barrier value $\ell(\ell+1)$. The actual value of C is fixed by the requirement that the logarithmic derivative (6) coincides at the mid point R_m with the ℓ=0 component of the HFB+HO density, i.e., with

$$\bar{\rho}(r) = \int_0^{\pi/2} \bar{\rho}(r,\theta) P_{\ell=0}(\cos(\theta)) \sin(\theta) d\theta. \tag{9}$$

Next, in order to make a smooth transition from the HFB+HO density $\bar{\rho}(r)$ in the inner region to the approximate asymptotic expression (6) in the outer region, we introduce the following approximation $\tilde{\rho}$ for the logarithmic density derivative:

$$\frac{\tilde{\rho}'(r)}{\tilde{\rho}(r)} = \begin{cases} \dfrac{\bar{\rho}'(r)}{\bar{\rho}(r)} & \text{for } r \le R_{\min} \\ a\dfrac{(R_{\min}-r)^2}{r^s} + b & \text{for } R_{\min} \le r \le R_{\max} \\ -\dfrac{2}{r} - 2\sqrt{\kappa^2+\mathcal{V}} - \dfrac{1}{2}\dfrac{\mathcal{V}'}{\kappa^2+V} & \text{for } r \ge R_{\max} \end{cases} \tag{10}$$

The coefficients a and b, and the power s, are determined from the condition that the logarithmic derivative (10) and its first derivative are smooth functions at the points $R_{\min}$ and $R_{\max}$. Note that the first derivative of (10) at $R_{\min}$ is automatically equal to zero, so that there is no need to introduce a fourth parameter to satisfy this condition.

Having determined the smooth expression for the logarithmic derivative of $\tilde{\rho}(r)$, we can derive the approximate local density distribution $\tilde{\rho}(r)$ by simply

integrating Eq. (10). The result is

$$\tilde{\rho}(r) = \begin{cases} \bar{\rho}(r) & \text{for } r \le R_{\min} \\ A\, e^{-b\,r} \exp\left[-\dfrac{a}{r^s}\left(\dfrac{a\,r^3}{3-s} - \dfrac{2\,r^2 R_{\min}}{2-s} + \dfrac{r\,R_{\min}^2}{1-s}\right)\right] & \text{for } R_{\min} \le r \le R_{\max} \\ B\,\dfrac{\exp\left[-2\int^r \sqrt{\kappa^2+\mathcal{V}}dr\right]}{r^2\sqrt{\kappa^2+\mathcal{V}}} & \text{for } r \ge R_{\max} \end{cases} \tag{11}$$

where the integration constants A and B are determined from the matching condition for the density at points $R_{\min}$ and $R_{\max}$, respectively. Finally, $\tilde{\rho}(r)$ should be normalized to the appropriate particle number.

The approximate density (11) works fairly well for all nuclei that we have considered. This is illustrated in Figure 1 where the approximate density $\tilde{\rho}$ (circles) is seen to be in perfect agreement with the coordinate-space HFB results.

It should be stressed that the above procedure is applicable only for such a number of shells for which HFB+HO density has a minimum at the point $R_{\min}$. This number could not be smaller than on certain value of $N_{\rm sh}$ which depends on particular deformations or nuclei considered. For the number of shells $N_{\rm sh} = 20$ used in our calculations the above condition is always satisfied.

3.3 LST Function for HFB+THO Calculations

The starting point of our new and improved HFB+THO procedure is thus to carry out a standard HFB+HO calculation for the nucleus of interest, thereby generating its local density and its local ℓ=0 density $\bar{\rho}(r)$ (9), and then to use the method outlined in the previous subsection to correct that density at large distances, see Eq. (11), by calculating $\tilde{\rho}(r)$. The next step is to define the LST [18] so that it transforms the HFB+HO ℓ=0 density (9) into the corrected density of Eq. (11). This requirement leads to the following first-order differential equation,

$$\tilde{\rho}(r) = \frac{f^2(\mathcal{R})}{\mathcal{R}^2}\frac{\partial f(\mathcal{R})}{\partial \mathcal{R}}\bar{\rho}\left(\frac{r}{\mathcal{R}}f(\mathcal{R})\right)\ , \tag{12}$$

which for the initial condition $f(0) = 0$ can always be solved for $f(\mathcal{R})$.

Once the LST function has been so obtained, we need simply diagonalize the HFB matrices in the corresponding THO basis. Most importantly, no information is required to build the THO basis beyond the results of a standard HFB+HO calculation. Since no further parameters enter, there is no need to minimize the HFB+THO total energy. As a consequence, with this new methodology we are able to systematically treat large sets of nuclei within a single calculation.

Despite the fact that the new HFB+THO method is simpler to implement than the earlier version, there are no discernible differences between the results obtained with the two distinct treatments of the LST function. Most importantly, the current formulation leads to the same excellent reproduction of coordinate-space results as did the previous one [18, 20].

4 Results

In this section, we present the results of HFB+THO calculations performed for all particle-bound even-even nuclei with $Z \leq 108$ and $N \leq 188$. The THO basis was implemented according to the general prescription developed in the previous section. The k value used in the procedure was obtained in the following way. From the starting HFB+HO calculation, we determine k values separately for neutrons and protons, using Eq. (5). We then associate the k value for the transformation with the smaller of k_p and k_n. In this way, the THO basis is always adapted to the less-bound type of particle. The calculations were performed by building THO basis states from spherical HO bases with oscillator frequencies of $\hbar\omega_0 = 1.2 \times 41\,\mathrm{MeV}\,/A^{1/3}$.

In order to meaningfully test predictions of nuclear masses for neutron-rich nuclei, we used the SLy4 Skyrme force parameterization [27], as this was adjusted with special emphasis on the properties of neutron matter. In the pairing channel, we used a pure volume contact pairing force $V^{\delta}(\mathbf{r}, \mathbf{r}') = V_0\delta(\mathbf{r} - \mathbf{r}')$ with strength V_0=-187.1 MeV fm^3($N_{sh} = 20$) and acting within a phase space limited by a cut-off parameter [18] of $\bar{e}_{\max}$=60 MeV.

For a given mass number A, calculations were carried out for increasing (decreasing) $N-Z$ up to the nucleus with positive neutron (proton) Fermi energy. Moreover, three independent sets of calculations were performed, for initial wave functions corresponding to oblate, spherical, and prolate shapes. The lowest of the local minima that were found for a given nucleus was then identified with the ground-state solution.

The results we obtained for ground-state quadrupole deformations β are illustrated in Figure 2 in the case of $N_{sh} = 14$. As in Ref. [18], the deformations were estimated from the total quadrupole moments and rms radii through a simple first-order expression. All even-even nuclei with negative Fermi energies, λ_n<0 and λ_p<0, are shown. Figure 3 shows similar results for the two-neutron separation energies S_{2n}. Table 4 summarizes in more detail our results for even-even nuclei along the two-particle drip lines with $N_{sh} = 20$. More specifically, for each value of Z, the results for the lightest isotope with λ_p <0, and the heaviest isotope with λ_n <0 are shown.

Table 1. Results of the HFB+THO calculations for drip-line nuclei with the SLy4 Skyrme force and volume delta pairing force within $N_{sh} = 20$ major shells.

Two-proton drip line						Two-neutron drip line					
Nucleus	β	λ_p	S_{2p}	Δ_n	Δ_p	Nucleus	β	λ_n	S_{2n}	Δ_n	Δ_p
^{4}He	0	-16.20		0	0	^{10}He	0	-0.65	-2.47	0	0
^{6}Be	0	-2.05	1.72	0	1.919	^{16}Be	0.445	-0.77	-1.23	0	0.006
^{8}C	0	-1.96	-1.37	0	0	^{22}C	0	-2.66	1.52	0	0
^{12}O	0	-2.11	1.20	1.994	0	^{28}O	0	-1.75	0.90	0	0
^{18}Ne	0	-3.19	6.35	0	1.563	^{34}Ne	0.322	-1.54	1.20	0	0.289
^{20}Mg	0	-1.78	3.20	0	1.483	^{44}Mg	-0.131	-0.54	-0.21	0	1.233
^{22}Si	0	-0.42	0.81	0	0.573	^{48}Si	0	-0.71	0.33	0	0
^{26}S	0	-1.56	1.69	1.578	0	^{52}S	-0.104	-0.68	-0.78	0.010	.886
^{30}Ar	-0.135	-0.24	-0.96	1.398	0.008	^{58}Ar	0	-2.17	1.86	0.002	1.026
^{34}Ca	0	-1.71	1.54	0	0	^{70}Ca	0	-1.31	0.21	0	0
^{40}Ti	-0.043	-0.74	1.68	1.055	1.043	^{74}Ti	0.121	-0.41	-0.62	0	0.838
^{44}Cr	0	-1.58	3.51	0	1.234	^{82}Cr	0	-0.29	-0.29	0	1.072
^{46}Fe	0	-0.55	1.36	0	1.045	^{84}Fe	0	-0.50	0.51	0	0.938
^{48}Ni	0	-0.70	-0.56	0	0	^{92}Ni	0.339	-0.07	0.03	0.498	0
^{54}Zn	0.207	-0.56	0.26	0.640	0	^{100}Zn	0.221	-0.04	-0.19	0.748	0
^{60}Ge	0	-1.20	1.54	0	0	^{108}Ge	0.156	-0.20	0.12	0.604	0.671
^{64}Se	-0.203	-1.23	1.09	0.741	0.004	^{116}Se	0	-1.87	0.34	0	1.020
^{70}Kr	-0.248	-0.84	2.31	0	0.764	^{118}Kr	0	-2.61	2.72	0	0.854
^{70}Sr	0.412	-0.19	-3.47	1.033	0	^{120}Sr	0	-3.29	4.42	0	0.483
^{74}Zr	0	-0.58	-0.23	1.267	0.003	^{122}Zr	0	-3.97	5.78	0	0.568

Table 1. – Continued

Two-proton drip line						Two-neutron drip line					
Nucleus	β	λ_p	S_{2p}	Δ_n	Δ_p	Nucleus	β	λ_n	S_{2n}	Δ_n	Δ_p
^{82}Mo	0	-0.62	1.83	0.036	0.854	^{132}Mo	0	-0.06	0.18	0.033	0.772
^{86}Ro	0	-0.79	2.10	0.996	0.987	^{136}Ro	0	-0.11	0.01	0.360	0.864
^{90}Pd	0.133	-0.86	2.70	0.795	0.442	^{150}Pd	-0.223	-0.06	0.34	0.344	0.541
^{92}Cd	-0.009	-0.11	-0.02	1.118	0.745	^{162}Cd	0	-0.18	0.25	1.001	0.620
^{94}Sn	0	-0.23	-0.93	1.118	0	^{176}Sn	0	-1.42	0.87	0	0
^{106}Te	0.158	-0.83	-0.26	0.702	0.001	^{178}Te	0	-2.03	2.04	0	0.663
^{112}Xe	0.215	-0.82	2.02	0.894	0.508	^{180}Xe	0	-2.51	3.13	0	0.804
^{114}Ba	0.237	-0.55	0.60	0.858	0.003	^{182}Ba	0	-2.82	4.17	0	0.818
^{116}Ce	0.466	-0.69	-1.52	0.014	0	^{186}Ce	0.441	-0.04	-15.40	0.585	0
^{120}Nd	0.388	-0.10	-0.29	0.009	0.001	^{188}Nd	0.364	-0.62	-14.62	0.781	0
^{130}Sm	0.351	-0.61	1.81	0.383	0.625	^{190}Sm	0.437	-0.87	-13.57	0.604	0.591
^{134}Gd	0.340	-0.65	1.78	0.030	0.686	^{194}Gd	0.062	-0.10	12.02	0.301	0.802
^{138}Dy	0.386	-0.10	1.01	0.017	0.376	^{216}Dy	-0.219	-0.05	0.03	0.656	0.580
^{144}Er	-0.195	-0.47	1.83	0.846	0.480	^{222}Er	0.284	-0.12	0.19	0.437	0.451
^{148}Yb	-0.166	-0.04	0.77	0.605	0.705	^{230}Yb	-0.210	-0.02	-5.26	0.655	0.167
^{152}Hf	0.431	-0.57	-7.50	0.912	0	^{236}Hf	-0.196	-0.15	0.28	0.561	0.478
^{158}W	-0.068	-0.47	1.42	0.624	0.975	^{252}W	-0.113	-0.40	-0.07	0.003	0.693
^{162}Os	0.117	-0.03	0.52	0.694	0.722	^{260}Os	0	-1.15	1.04	0	0.854
^{168}Pt	0.139	-0.03	0.45	0.859	0.556	^{262}Pt	0	-1.36	1.62	0	0.729
^{170}Hg	-0.098	-0.19	-0.79	1.145	0.002	^{264}Hg	0	-1.58	2.29	0	0.514
^{172}Pb	0	-0.24	-0.77	1.312	0	^{266}Pb	0	-1.83	2.98	0	0

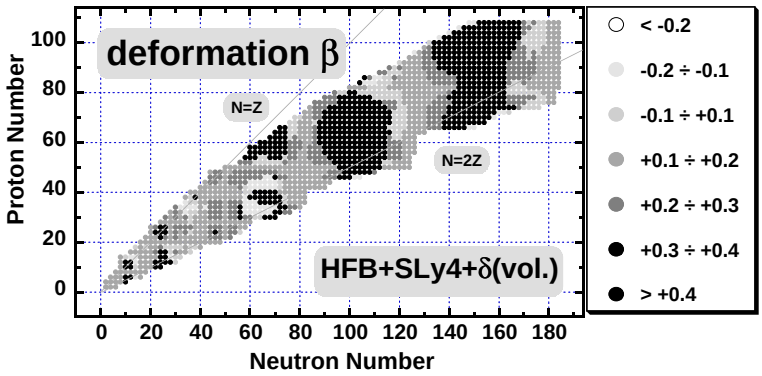

Figure 2. Quadrupole deformations of particle-bound even-even nuclei calculated within the HFB+THO method for the Skyrme SLy4 interaction and volume contact pairing force within $N_{sh} = 14$ major shells.

It is interesting to note from Figure 2 that there are fairly large regions of nuclei far from stability with oblate shapes in their ground state. Nonetheless, it remains the case for nuclei far from stability as for nuclei in or near the valley of stability that there are more prolate ground states than oblate.

From Table 1, we see that there exist numerous particle-bound even-even nuclei (i.e., nuclei with negative Fermi energies) that at the same time have negative two-proton or two-neutron separation energies. What this means is that even though these nuclei are bound against one-nucleon emission they can nevertheless decay spontaneously by two-nucleon emission. Such an effect was already noticed in light nuclei in Ref. [18]. It is related to the fact that the Fermi ener-

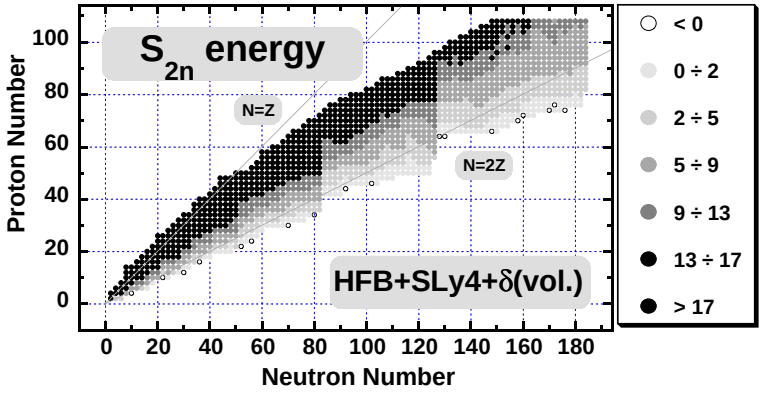

Figure 3. Same as in Figure 2 but for the two-neutron separation energies.

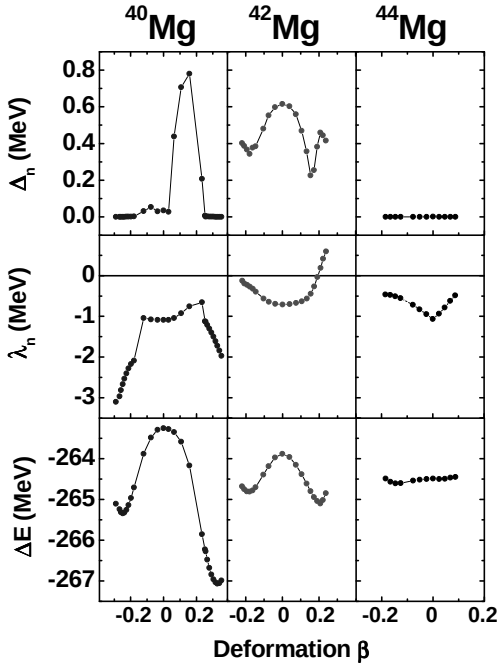

Figure 4. Neutron pairing gaps Δ_n (upper panels) and Fermi energies λ_n (middle panels) as well as the total binding energies (lower panels) calculated in ^{40}Mg, ^{42}Mg, and ^{44}Mg as functions of the quadrupole deformation β.

gies pertain to the stability with respect to particle emission of a given configuration or shape, namely that of the ground state. In all of the cases in which this phenomenon is seen, (a) the neighboring even-even nucleus (the one to which it decays by two-nucleon emission) has two distinct shapes with negative Fermi energies, (b) its ground state shape is different than that of the parent nucleus, and (c) decay to its excited configuration, the configuration with the same shape as the parent, is energetically forbidden.

Among the many such cases that appear along the two-neutron drip line, we focus here on the heaviest isotopes of magnesium and selenium [see Figures 4 and 5, respectively]. The figures show the neutron pairing gaps Δ_n, Fermi energies λ_n and total binding energies obtained in constrained HFB+THO calculations as a function of the quadrupole deformation β in the last three particle-bound isotopes of the two isotopic chains. For each, the binding energies of the last three isotopes are shown on a common energy scale. In ^{40}Mg the neutron Fermi energies λ_n have negative values for all deformations, so that the configurations for all deformations are particle-bound. In these nuclei, minima arise for both oblate and prolate shapes, with the prolate shape being lowest. The same

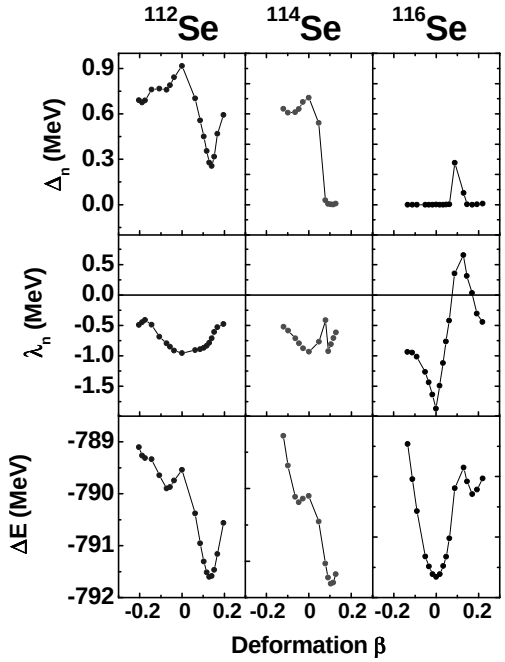

Figure 5. Same as in Figure 4 but for ^{112}Se, ^{114}Se, and ^{116}Se.

is also true for the next nucleus ^{42}Mg but the prolate minimum has a positive λ_n value and such a minimum must be disregarded since it does not correspond to a localized HFB state. Therefore, the ground state deformation changes from prolate ^{40}Mg to oblate in ^{42}Mg. In ^{44}Mg, neutron pairing disappears and neutron fermi energies have negative values again. The lowest minimum in this case shows an oblate deformation as well. It is clear from Figure 4 that in ^{42}Mg the two-neutron separation energy is negative, however, since ^{42}Mg and ^{40}Mg have different shapes in their ground states, the real process of emitting two neutrons may be hindered, and the lifetime of ^{42}Mg could be larger than expected. A similar situation occurs in ^{116}Se when compared to ^{114}Se, as can be readily seen from Figure 5.

5 Concluding Remarks

In this paper, we report the development of an improved version of the configuration-space HFB method expanded in a Transformed Harmonic Oscillator basis. In its current form, the method can be used reliably in systematic studies of wide ranges of nuclei, both spherical and axially deformed, extending all the way out to nucleon drip lines. The key step was the development of a pre-

scription for choosing a reliable transformation function to define the THO basis that does not require variational optimization. The current prescription only involves information from a preliminary configuration-space HFB calculation carried out in a harmonic oscillator basis. The transformation function is then tailored to correct the asymptotic properties of the HFB+HO results. The resulting HFB+THO theory accurately reproduces results of coordinate-space HFB theory, where available, and also reproduces the results obtained with an earlier version of the transformation that had to be optimized separately for each nucleus.

As a first application of the new HFB+THO methodology, we carried out a systematic study of all even-even nuclei having $Z \leq 108$ and $N \leq 184$. We focussed our discussion here on those nuclei that are very near the nucleon drip lines, finding that in several regions of the periodic table there exist nuclei that are stable against one-particle emission but unstable against pair emission. We showed that invariably this is associated with a shape change in the ground state. Thus, while two-particle emission to the configuration of the daughter with the same shape as the parent is forbidden in these nuclei, spontaneous decay to the ground state can nevertheless occur. The change in shape associated with these spontaneous pair emissions may conceivably lead to sufficient hindrance of the decays so that the corresponding nuclei that formally live beyond the drip lines can be observed experimentally. This phenomenon, which had earlier been noted in calculations of light nuclei, is now seen to be a more common feature of nuclei near the drip lines.

In the description of very weakly-bound systems, small changes in results can have important consequences, determining for example the precise location of the drip lines. Thus, it is important to continue to improve the current HFB+THO methodology to accommodate effects not presently being included. Particularly important is the restoration of symmetries, either exact or approximate. Also important is to develop the new HFB+THO formalism for application to odd-mass systems, including the effects of Pauli blocking. Work along these various lines is currently underway.

Acknowledgments

This work has been supported in part by the Bulgarian National Foundation for Scientific Research under project Φ-809, by the Polish Committee for Scientific Research (KBN) under Contract No. 5 P03B 014 21, by the U.S. Department of Energy under Contract Nos. DE-FG02-96ER40963 (University of Tennessee), and DE-AC05-00OR22725 with UT-Battelle, LLC (Oak Ridge National Laboratory), by the US National Science Foundation under grant # PHY-9970749, and by the computational grants from the *Regionales Hochschulrechenzentrum Kaiserslautern* (RHRK), Germany, and from the Interdisciplinary Centre for Mathematical and Computational Modeling (ICM) of the Warsaw University.

References

[1] E. Roeckl, (1992) *Rep. Prog. Phys.* **55** 1661.

[2] A. Mueller and B. Sherril, (1993) *Annu. Rev. Nucl. Part. Sci.* **43** 529 .

[3] P.-G. Hansen, (1993) *Nucl. Phys.* **A553** 89c.

[4] J. Dobaczewski and W. Nazarewicz, (1998) *Phil. Trans. R. Soc. Lond.* **A356** 2007.

[5] A. Bulgac, (1980) *Preprint FT-194-1980*, Central Institute of Physics, Bucharest, *nucl-th/9907088*.

[6] J. Dobaczewski, H. Flocard, and J. Treiner, (1984) *Nucl. Phys.* **A422** 103.

[7] J. Dobaczewski, W. Nazarewicz, T.R. Werner, J.-F. Berger, C.R. Chinn, and J. Dechargé, (1996) *Phys. Rev.* **C53** 2809.

[8] J. Terasaki, H. Flocard, P.-H. Heenen, and P. Bonche, (1997) *Nucl. Phys.* **A621** 706.

[9] N. Tajima, (1998) *XVII RCNP International Symposium on Innovative Computational Methods in Nuclear Many-Body Problems*, (eds. H. Horiuchi *et al.*; World Scientific, Singapore) p. 343.

[10] V.E. Oberacker and A.S. Umar, (1999) *Proc. Int. Symp. on Perspectives in Nuclear Physics*, (World Scientific, Singapore), Report *nucl-th/9905010*.

[11] J. Terasaki, P.-H. Heenen, H. Flocard, and P. Bonche, (1996) *Nucl. Phys.* **A600** 371.

[12] D. Gogny, (1975) *Nucl. Phys.* **A237** 399.

[13] M. Girod and B. Grammaticos, (1983) *Phys. Rev.* **C27** 2317.

[14] J.L. Egido, H.-J. Mang, and P. Ring, (1980) *Nucl. Phys.* **A334** 1.

[15] J.L. Egido, J. Lessing, V. Martin, and L.M. Robledo, (1995) *Nucl. Phys.* **A594** 70.

[16] A.V. Afanasjev, J. König, and P. Ring, (1996) *Nucl. Phys.* **A608** 107.

[17] P. Ring, (1996) *Prog. Part. Nucl. Phys.* **37** 193.

[18] M.V. Stoitsov, J. Dobaczewski, P. Ring, and S. Pittel, (2000) *Phys. Rev.* **C 61** 034311.

[19] M.V. Stoitsov, P. Ring, D. Vretenar, and G.A. Lalazissis, (1998) *Phys. Rev.* **C58** 2086.

[20] M.V. Stoitsov, W. Nazarewicz, and S. Pittel, (1998) *Phys. Rev.* **C58** 2092.

[21] I.Zh. Petkov and M.V. Stoitsov, (1981) *Compt. Rend. Bulg. Acad. Sci.* **34** 1651; (1983) *Theor. Math. Phys.* **55** 584; (1983) *Sov. J. Nucl. Phys.* **37** 692.

[22] M.V. Stoitsov and I.Zh. Petkov, (1988) *Ann. Phys.* (NY) **184** 121.

[23] I.Zh. Petkov and M.V. Stoitsov, (1991) *Nuclear Density Functional Theory*, Oxford Studies in Physics, (Clarendon Press, Oxford).

[24] P. Ring and P. Schuck, (1980) *The Nuclear Many-Body Problem* (Springer-Verlag, Berlin).

[25] F. Pérez-Bernal, I. Martel, J.M. Arias, and J. Gómez-Camacho, (2001) *Phys. Rev.* **A63** 052111.

[26] A. Messiah, (1962) *Quantum Mechanics* vol I (Wiley, New York).

[27] E. Chabanat, P. Bonche, P. Haensel, J. Meyer, and F. Schaeffer, (1998) *Nucl. Phys.* **A635** 231.